Hindawi
International Transactions on Electrical Energy Systems
Volume 2022, Article ID 4218067, 12 pages
https://doi.org/10.1155/2022/4218067

WILEY | Hindawi

Research Article

A Robust Controller Design for Load Frequency Control in Islanded Microgrid Clusters

Mohammad Reza Ghodsi[1] **Alireza Tavakoli**[2] **and Amin Samanfar**[1]

[1]*Department of Electrical Engineering, Khorramabad Branch, Islamic Azad University, Khorramabad, Iran*
[2]*Department of Electrical Engineering, Ahvaz Branch, Islamic Azad University, Ahvaz, Iran*

Correspondence should be addressed to Alireza Tavakoli; a.tavakoli@iauahvaz.ac.ir

Received 8 January 2022; Revised 6 April 2022; Accepted 5 May 2022; Published 16 August 2022

Academic Editor: Salvatore Favuzza

In this paper, virtual inertia control (VIC) is suggested to increase the frequency stability in islanded microgrid (MG) clusters. The aim of the suggested control method is to improve damping characteristic of MG clusters including different distributed generations (DGs). The optimal/robust values of the VIC parameters are tuned by a μ-synthesis robust control method. The proposed robust/optimal VIC-based control method is confirmed by various scenarios. Computer simulation and hardware-in-the-loop (HIL) tests are used to show the effectiveness of the suggested method in increasing the damping of the power system. Clearly, different characteristics of the dynamic responses and the results show the practicality of the suggested robust VIC.

1. Introduction

The main task of load frequency controllers (LFCs) is to remove frequency deviations and, consequently, to adjust the system frequency following unexpected disturbances/changes [1–4]. It is well known that the energy stored in the rotor inertia of synchronous generators (SGs) contributes significantly to maintaining the stability of the system during faults. In this regard, the frequency/voltage of power systems must be stabilized and well tuned. Today, renewable energy sources (RESs) are rapidly integrating into traditional power systems. Future plans show a crucial role for RESs around the world. These RESs and distributed generators (DGs) reduce the total inertia of the power system due to their low stored inertia.

In recent studies, a virtual implementation of SG behavior with modeling and simulation is suggested to achieve system stability and compensate for system inertia [5–8]. In recent years, research has been conducted to investigate the concept of virtual inertia control to deal with the negative effects of RESs on the stability of power systems [3–6]. In [9], to increase the system inertia, a cascade control scheme using permanent-magnet synchronous generator (PMSG) wind turbines is suggested.

In [10], by shifting the operating point of the wind turbine from the maximum power point (MPP) to the VIC curves in relation to the frequency deviation, the damping capabilities and inertial dynamic responses during faults are improved. In [11, 12], the idea of droop control for virtual inertia is expressed on wind turbines to improve the dynamic responses of the power system. In [13], the authors implemented the grid-side converter to support frequency and voltage regulation. In [14], a VIC using H_∞ method is proposed to improve the frequency stability of an MG. In [15–18], double fed induction generator (DFIG)-based wind turbines are used as a virtual synchronous generator to improve system dynamic responses. In [19], adaptive VIC is proposed to increase frequency stability. In this method, the VIC's parameters are updated by the frequency deviation. A virtual synchronous generator (VSG) based on a bang-bang control strategy is proposed in [20]. In this method, the stability analysis of the system is performed by a small signal model. To obtain a desired dynamic response, an adaptive approach is proposed in [21] for a VSG in which a relatively

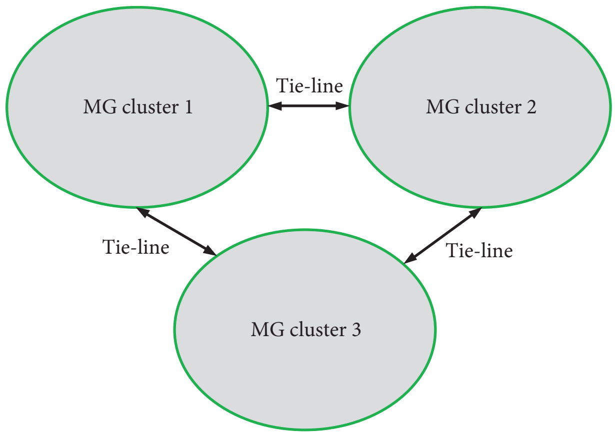

Figure 1: The islanded multiple AC microgrid clusters under study.

complex mathematical algorithm is obtained to realize an adaptive mechanism for updating the inertia parameter of the VSG. The main drawback of these methods is that they depend on the accuracy of the mathematical model.

In several papers, optimization algorithms such as genetic slgorithm (GA) [22], particle swarm optimization (PSO) [23], grey wolf optimization (GWO) [24], Harris's hawk optimization [25], and firefly [26] have been proposed to improve the frequency stability of microgrids. The nonrobust performance can be considered as the most important problem of these methods.

Most published research studies focused on the study of virtual inertia control performance in a single small-scale microgrid, and there are no reports focusing on virtual inertia control for a large-scale microgrid involving a number of clusters. A real microgrid may consist of a number of clusters, each with a number of high-penetration DGs. In this case, the virtual controller may not work properly and may need to be redesigned.

In this study, virtual inertia control is proposed to increase frequency stability of MG clusters. To control the frequency and enhance the inertia of the MG clusters, the suggested VIC is applied to the inverter-based DGs as a virtual inertia controller. The main features of the suggested method are summarized below:

(i) The suggested VIC emulates damping and the inertia feature, and frequency control loops characteristics of synchronous generators. Combining the virtual rotor and virtual primary and secondary controllers utilized in the synchronous generators, the suggested method can compensate the lack of inertia in the MG clusters.

(ii) To robustly and optimally tune the VIC's parameters, a μ-synthesis method is used. Therefore, uncertainties existing in the MG system can be easily addressed by the suggested method.

(iii) The suggested VIC can provide the required inertia for the MG system to improve the frequency stability under serious faults and uncertainties.

(iv) In the structure of the suggested VIC, there are both the inertial response characteristics of original synchronous generator and the fast dynamics of power electronic interfaces. This leads to great flexibility in designs.

2. Modeling of the Microgrid

Figure 1 shows the islanded multiple AC microgrid clusters studied in this paper. Each MG has a number of DGs, and the MGs are connected to each other via a tie line. In the first MG, a photovoltaic panel (PV), a diesel engine generator (DEG), and a fuel cell (FC) are employed. In the second MG, there are a fuel cell, a wind turbine generator (WTG), and a diesel engine generator. The third MG includes a photovoltaic panel, a flywheel energy storage system (FESS), and a diesel engine generator.

To achieve voltage conversion or synchronization between DC and AC systems, a power electronic interface and interconnection equipment (IC) are used. FC and PV need proper power converters for energy exchange with AC systems.

Due to the dependence of the power generated by WTGs and PVs on environmental conditions, they play no role in frequency control. Therefore, the secondary loop control (ΔP_{SL}) is applied to the DEG. Fluctuations in PV, WTG, and load and uncertainty in MG, on the one hand, and low inertia of inverters, on the other hand, negatively affect the performance of frequency controllers. To tackle this problem, the suggested VIC designed by μ-synthesis is applied to the inverter of the PV system in clusters 1 and 2 and the fuel cell in cluster 2. Figures 2(a)–2(c) present the dynamic model of the MG clusters, and parameters for each block are presented in Table 1.

The exchanged tie line power in each cluster is computed by

$$\begin{aligned}\Delta P_{\text{tie1}} &= \frac{2\pi T_{12}}{s}\left(\Delta f_1 - \Delta f_2\right) + \frac{2\pi T_{13}}{s}\left(\Delta f_1 - \Delta f_3\right),\\ \Delta P_{\text{tie2}} &= \frac{2\pi T_{21}}{s}\left(\Delta f_2 - \Delta f_1\right) + \frac{2\pi T_{23}}{s}\left(\Delta f_2 - \Delta f_3\right),\\ \Delta P_{\text{tie3}} &= \frac{2\pi T_{31}}{s}\left(\Delta f_3 - \Delta f_1\right) + \frac{2\pi T_{32}}{s}\left(\Delta f_3 - \Delta f_2\right),\end{aligned} \tag{1}$$

where T_{ij} is the tie line synchronizing torque coefficient between cluster i and cluster j.

3. Virtual Inertia Control

In the virtual inertia control, the power of inverter-based DGs is governed by the grid frequency derivation. Therefore, the lack of inertia is virtually compensated to improve the dynamic response of the MG. Distributed generators such as photovoltaic panels, fuel cells, batteries, and so on are connected to the power grid via DC/AC inverters. The inertia of the inverter-based DGs is much lower than that of synchronous generators having rotating parts. Increasing penetration of distributed power generation devices in

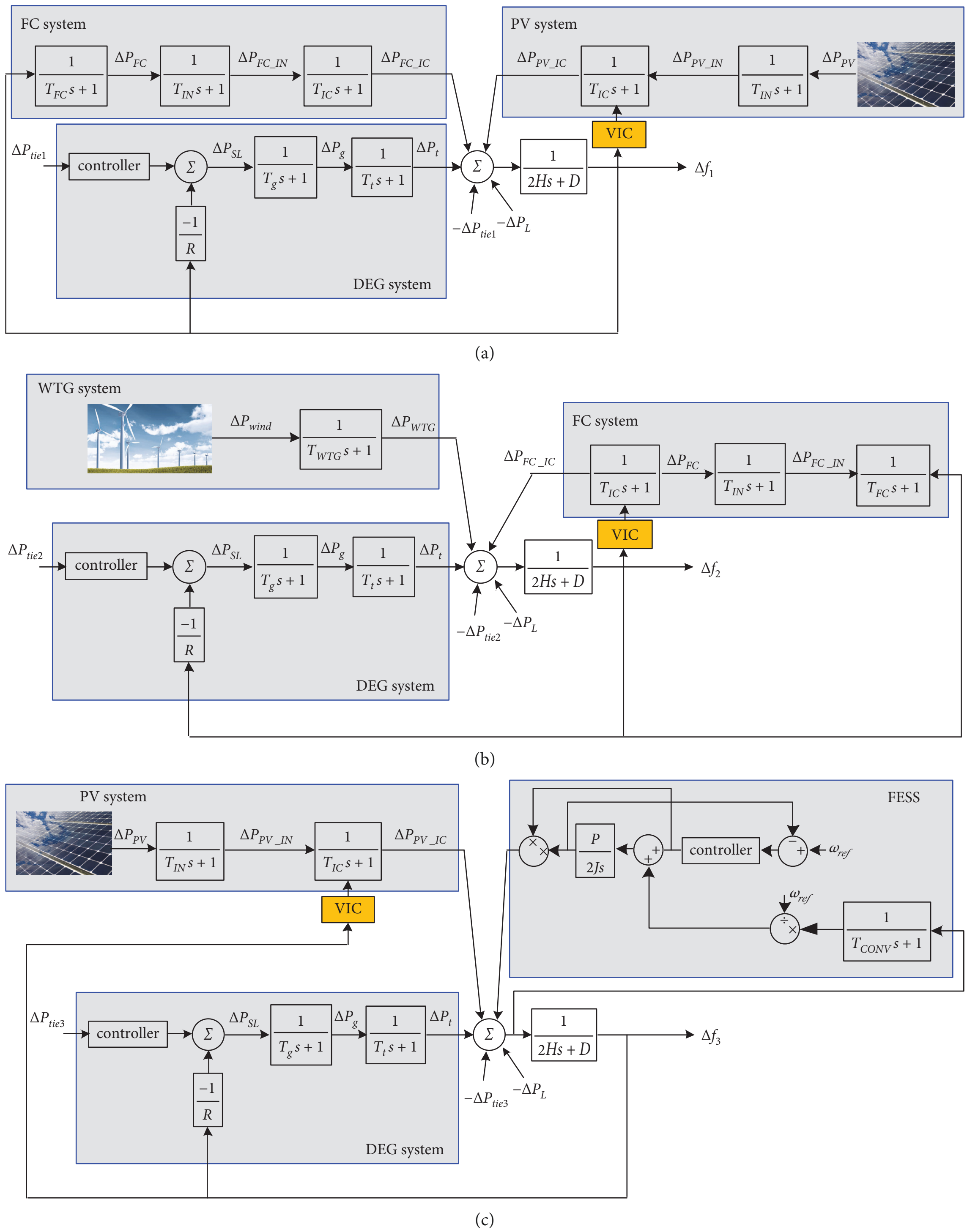

Figure 2: The dynamic model of the MGs: (a) cluster 1, (b) cluster 2, and (c) cluster 3.

recent years has reduced the total inertia of the power system. As a result, grid frequency oscillations cannot be efficiently damped out, and therefore, the power system stability is seriously threatened [6, 27, 28]. Additional inertia can be considered as a strategy to stabilize such a power system. In this regard, the concept of the virtual inertia control has been introduced in [29–32].

The following equation presents amount of emulated power to compensate the lack of inertia:

$$P_{\text{emu}} = K_{PE} f_o \frac{\mathrm{d}(\Delta f_i)}{\mathrm{d}t}, \tag{2}$$

where K_{PE} is the gain of the power electronics and f_o is the system frequency.

Table 1: Parameters of MG system.

Parameter	Value	Parameter	Value
D (pu/Hz)	0.012	T_{DEG} (s)	2
H (pu/s)	0.1	T_{WTG} (s)	1.5
T_{FC} (s)	4	T_{IN} (s)	0.08
T_{FESS} (s)	0.1	T_{IC} (s)	0.004
T_t	0.4	T_g	0.08
T_{conv}	0.1	P	4
J	2		

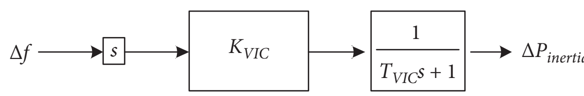

Figure 3: The block diagram of EVIC.

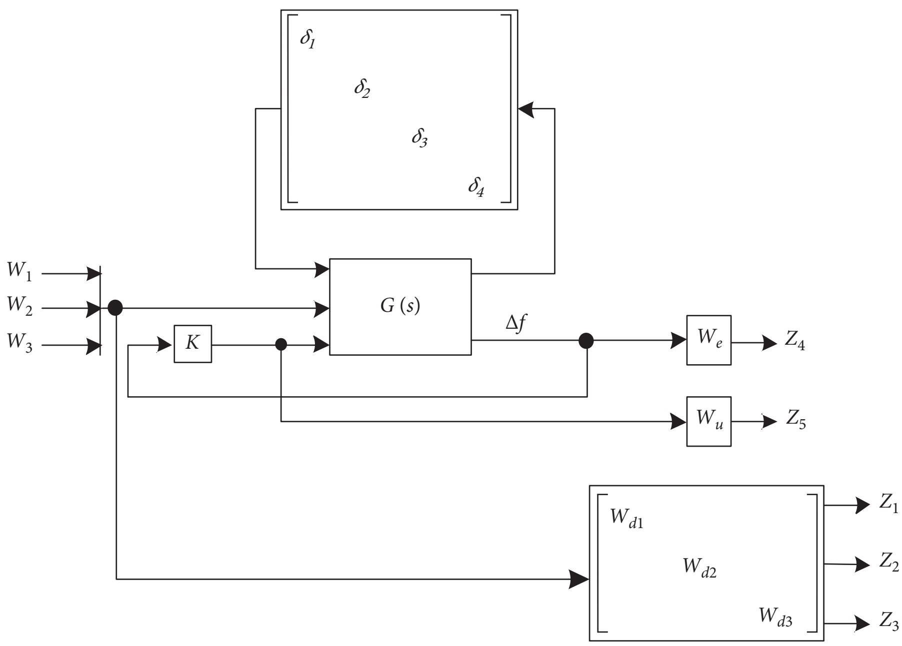

Figure 4: The block diagram of the closed-loop system along with uncertainty block.

Virtual inertia control is applied as a supplement to reduce frequency deviations in an interconnected grid in the presence of traditional automatic generation control (AGC). The virtual inertia control can be designed according to the concept of derivative control as follows:

$$\Delta P_{\text{inertia}} = \frac{K_{VIC}}{1 + sT_{VIC}} \frac{\mathrm{d}(\Delta f_i)}{\mathrm{d}t}, \quad (3)$$

where T_{VIC} and K_{VIC} are the time constant and gain of the VIC. Figure 3 shows the block diagram of the VIC. As shown in Figure 3, the frequency derivative is selected as the input of the VIC to reduce the frequency deviation during the penetration of renewable power and/or operating conditions.

4. μ-Synthesis Robust Control

The goal of this section is to design μ-synthesis robust control for the VIC. In this section, μ-synthesis theorem is used to robustly design K_{VIC}.

4.1. Modeling of Uncertainties. There are several definitions of the uncertainty modeling in the literature [33]. Generally, there are two categories for the uncertainty as dynamic perturbation: (1) modeling errors and (2) unmodeled dynamics.

For μ-synthesis, a single perturbation block Δ (s) referred to as "unstructured uncertainty" is considered as a lumped dynamic parametric perturbation. The structured uncertainty may contain parametric perturbation and structured unmodeled dynamics. The system dynamics can be used to extract the structured uncertainty block Δ shown in the general form of (2). Hence, a standard configuration of upper linear fractional transformation (LFT) can be used to rearrange the whole system. In this study, for simplification, only four parameters T_{FC}, T_t, T_g, and T_{WTG} are assumed to be subject to ± 25% uncertainty around their nominal values. Figure 4 shows the uncertainty "pulled out" of the loop for these four blocks of the MG system where T_c is constant time of these blocks and ΔT_c is its uncertainty. Besides, Δf is selected as the measured system output, and ΔP_{wind}, ΔP_{PV}, and ΔP_L are counted as disturbance signals.

The closed-loop block diagram of the microgrid along with a structured diagonal uncertainty is drawn in Figure 5. Here, a 4×4 parametric diagonal uncertainty is selected:

$$\Delta = \left\{\text{diag}\left[\delta_1 I_{r1}, \ldots, \delta_k I_{rk}, \ldots, \Delta_1, \ldots, \Delta_f\right], \delta_i \in C, \Delta_j \in C^{k_i \times k_j}\right\}. \tag{4}$$

4.2. D-K Iteration. To guarantee the robust performance of a dynamic system, the structured singular value (μ-based control) framework is used. The following equation is used to define μ function:

$$\mu_\Delta(M) = \frac{1}{\min\{\overline{\sigma}(\Delta)\colon |I - M\Delta| = 0, \Delta \in \Delta\}}. \tag{5}$$

Figure 6 illustrates the standard schematic of M-Δ configuration. In this figure, W represent the disturbance inputs, u represent the control signals, z represent the performance signals, y represent the measured outputs, and pert_{in} and pert_{out} are the input and output perturbation signals of the uncertain block. To satisfy the robust performance condition in μ-synthesis, $\|T_{wz}\|\infty \leq 1$ must be satisfied for all $\Delta \in \Delta_P$, where Δ_P is represented by

$$\Delta_P \coloneqq \left\{\begin{bmatrix} \Delta & 0 \\ 0 & \Delta_F \end{bmatrix}\colon \Delta \in R^{4\times 4}, \Delta_F \in C^{4\times 5}\right\}, \tag{6}$$

where Δ_F and Δ represent performance requirements and uncertainty, respectively. The robust performance will be guaranteed, if and only if

$$\max_{\omega} \mu_{\Delta_P}(M(s)). \tag{7}$$

The standard analytical method is unable to compute the μ-optimal controller presented in (7). So, equation (7) can be solved by a numerical method called D-K iteration [33]. This method determines controller K by minimizing the following equation:

$$\min_K\left(\min_{D(j\omega)} \left\|D(j\omega)M(K(j\omega))D^{-1}(j\omega)\right\|_\infty\right). \tag{8}$$

To design robust μ-controller, the LFT arrangement shown in Figure 7 is used to implement the D-K iteration method. In this figure, W_e (s), W_u (s), W_{d1} (s), W_{d2} (s), and W_{d3} (s) are the weighting functions to improve the robust performance and robust stability; w_1, w_2, and w_3 are disturbance inputs; u denotes the control signal; $z_{1\text{-}5}$ are

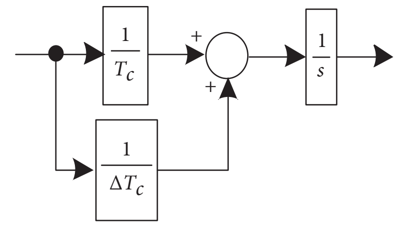

Figure 5: A block with uncertainty pulled out of the loop.

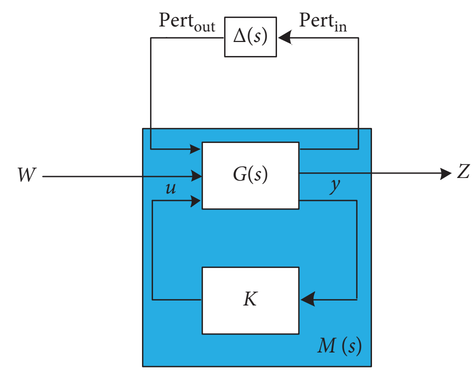

Figure 6: Standard schematic of M-Δ configuration.

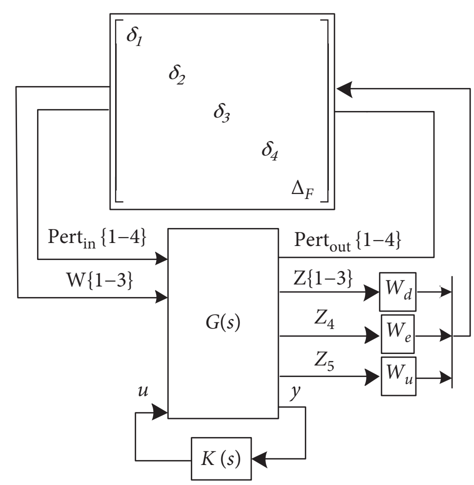

Figure 7: Block diagram of D-K iteration method.

desired performance signals; and y is the measured output. Here the weighting functions are chosen as follows:

$$W_e = \frac{0.005s^3 + 0.05s^2 + 50s + 125}{s^3 + 100s^2 + 300s + 1},$$
$$W_u = \frac{5s + 50}{s^2 + 3000s + 2 \times 10^4}, \tag{9}$$
$$W_d = 0.01 I_{3\times 3},$$

where I is the identity matrix.

In the D-K iteration method, the left-hand side value of (14) is alternately minimized for D and K while holding the other one fixed.

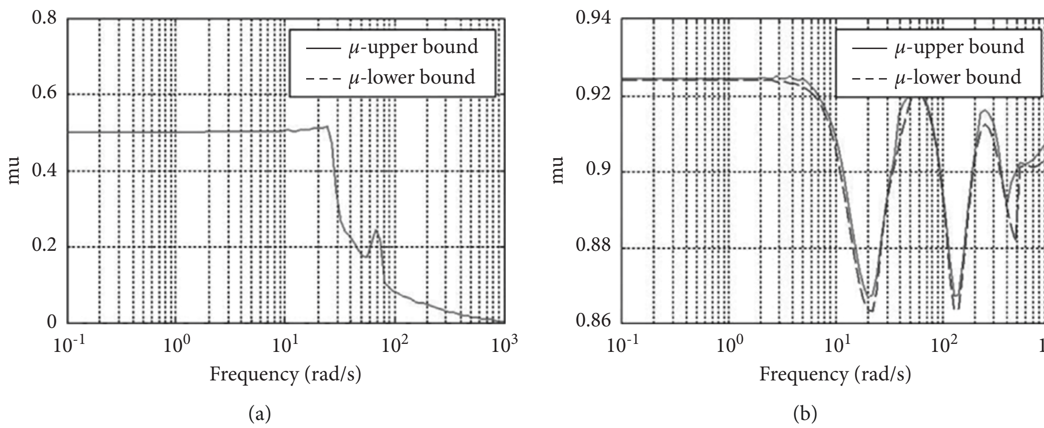

FIGURE 8: (a) The robust stability. (b) The robust performance.

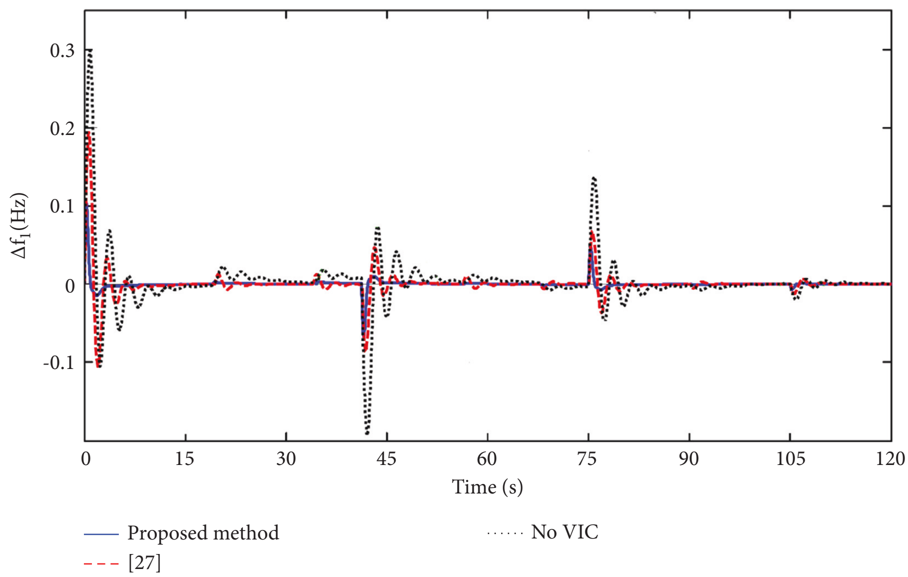

FIGURE 9: The frequency deviation in cluster 1.

4.3. Evaluating Robust Stability and Robust Performance. Two theorems called robust performance and robust stability can be defined by using the μ-synthesis method [33]. When a closed-loop system is internally stable, both robust performance and robust stability are met for any system with any uncertainty.

For the robust stability, considering $M{-}\Delta$ configuration, we can write

$$\Delta^* = \{\Delta(s_0) \in \Delta^*, s_0 \in C, \mathrm{Re}(s_0) \ge 0\},$$
$$M\begin{bmatrix} M_{11} & M_{12} \\ M_{21} & M_{22} \end{bmatrix}, \tag{10}$$

where $F_L(G,K)$ is the transfer function of the closed-loop system. For$\Delta \in \Delta^*$ and $\|\Delta\|_\infty \le 1$, the closed-loop system is internally stable when

$$\sup \mu_\Delta (M_{11}) \le 1. \tag{11}$$

For the robust performance, considering $M{-}\Delta$ configuration, we can write

$$\Delta_T = \left\{ \begin{bmatrix} \Delta_u & 0 \\ 0 & \Delta_p \end{bmatrix}, \Delta_u \in \Delta^*, \Delta_p \in C \right\}, \tag{12}$$

where Δ_p and Δ_u are performance and uncertainty requirements, respectively. For $\Delta \in \Delta_T$ and $\|\Delta\|_\infty \le 1$, the robust performance of the closed-loop system is guaranteed if and only if

$$\sup \mu_\Delta (M) \le 1. \tag{13}$$

Figure 8 shows the changes in μ versus frequency changes. From this figure, it is clear that at all frequencies, the value of μ-upper band is below 1, i.e., the system achieves robust performance.

5. Results and Discussion

This section presents the simulation and HIL results for some scenarios. The simulation tests are performed using MATLAB/Simulink under several load/RES perturbations.

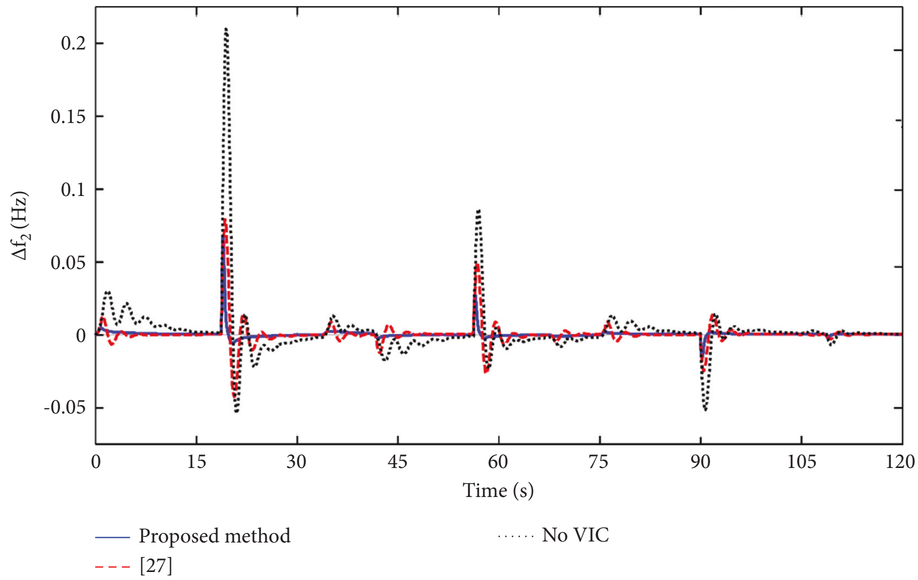

Figure 10: The frequency deviation in cluster 2.

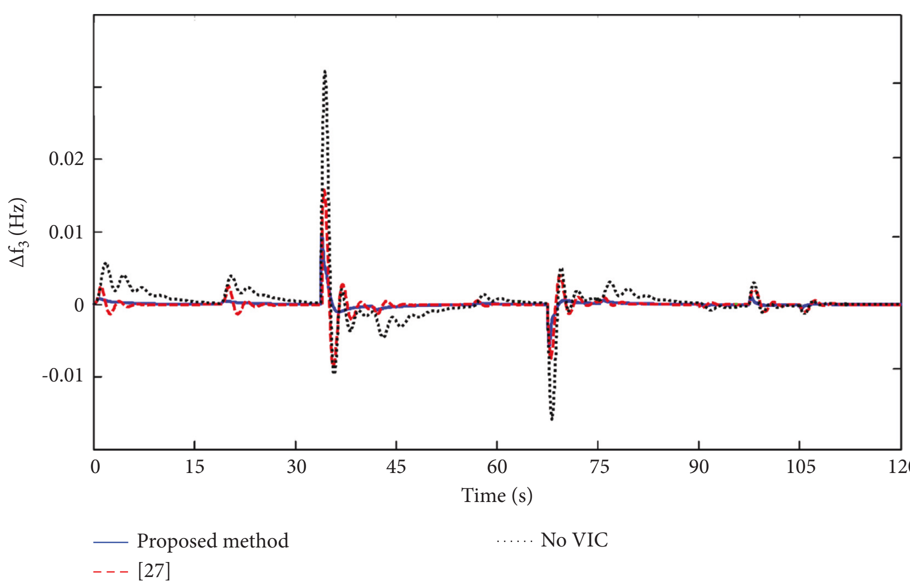

Figure 11: The frequency deviation in cluster 3.

Also, to show the effectiveness of the suggested VIC in low-inertia microgrids, the performance of the suggested VIC is compared with the method proposed in [6]. In [6], a virtual inertia has been used in a microgrid for the load frequency controller. A multiobjective optimization problem has been used to tune the parameters of MG.

To obtain the robust K_{VIC} using the μ-synthesis method, the D-K method is performed. The best robust performance is obtained after six iterations in the D-K method. The control transfer function obtained by the μ-synthesis method has an order of 28 which must be reduced for real-time implementation. In this paper, the Hankel-norm approximation method is used to reduce the order of the controller transfer function. The reduced controller transfer function is represented by

$$K_{VIC}(s) = \frac{n_5 s^5 + n_4 s^4 + n_3 s^3 + n_2 s^2 + n_1 s + n_0}{s^6 + d_5 s^5 + d_4 s^4 + d_3 s^3 + d_2 s^2 + d_1 s + d_0}, \tag{14}$$

where $n_0 = 5.14 \times 10^{20}$, $n_1 = 2.06 \times 10^{20}$, $n_2 = 9.19 \times 10^{16}$, $n_3 = 9.51 \times 10^{14}$, $n_4 = 2.03 \times 10^{10}$, $n_5 = 0.65 \times 10^{7}$, $d_0 = 6.28 \times 10^{16}$, $d_1 = 3.93 \times 10^{16}$, $d_2 = 9.88 \times 10^{14}$, $d_3 = 5.84 \times 10^{9}$, $d_4 = 7.38 \times 10^{8}$, and $d_5 = 7.66 \times 10^{4}$.

5.1. Simulations. In this section, simulation results are presented. The main purpose is to evaluate the performance of the proposed VIC considering the level of RES penetration, uncertainties, and nonlinearities in different areas. The microgrid is tested with heavy load changes in areas 1, 2, and 3. The frequency response of the microgrid clusters and

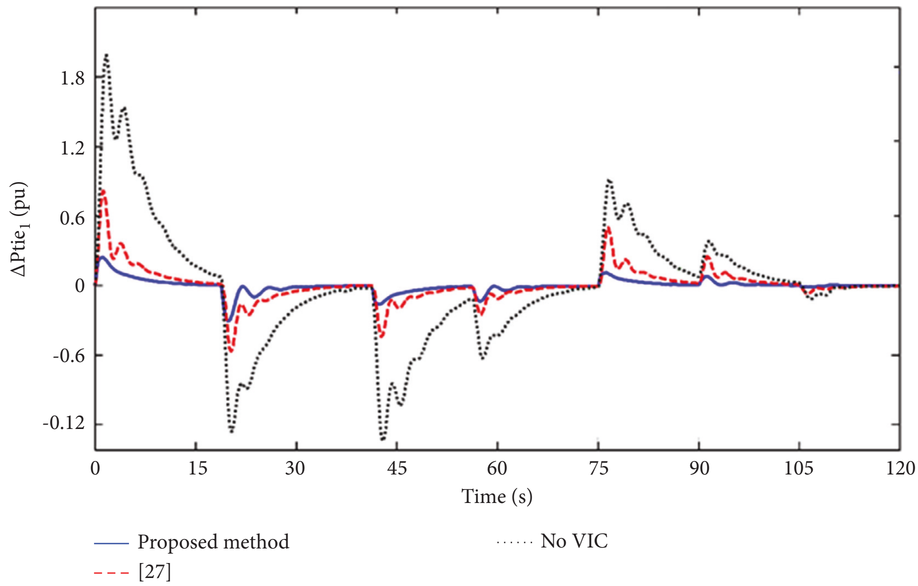

FIGURE 12: The tie line power deviation between cluster 1 and cluster 2.

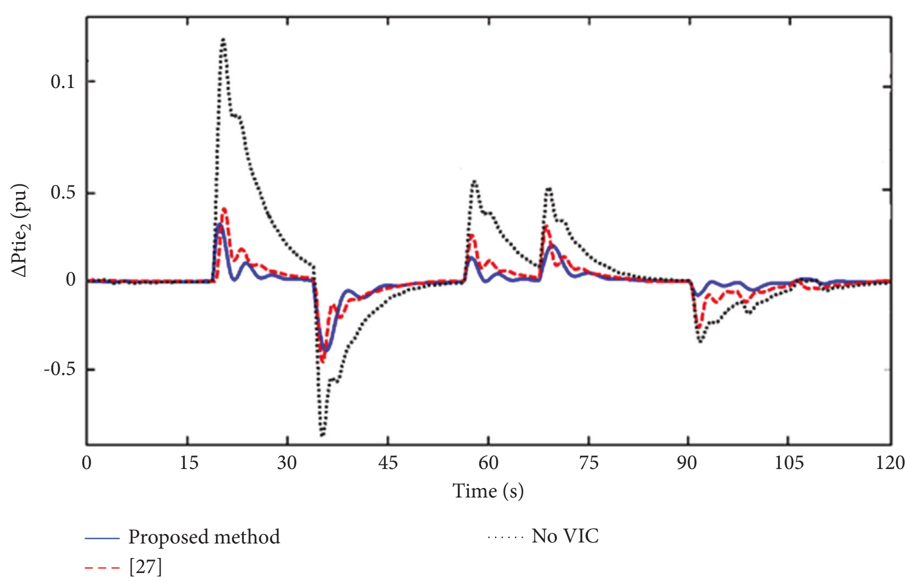

FIGURE 13: The tie line power deviation between cluster 2 and cluster 3.

tie line power deviation under heavy loading and penetration of RESs is drawn in Figures 9–14. When a decreasing load step occurs in one of the regions, the excess power leads to a positive frequency deviation, or in other words, the frequency increases in the microgrid clusters. Conversely, when an incremental load step occurs in one of the regions, the power shortage leads to a negative frequency deviation in all clusters, or in other words, the frequency decreases in microgrid clusters. In all these cases, the controller must quickly compensate for the positive or negative frequency deviation in the microgrid. In addition, the controller must damp frequency oscillations quickly and reduce frequency settling time. As can be seen in these figures, the suggested μ-synthesis-based VIC provides a better performance than the VSG proposed in [6], since the suggested method creates less frequency deviation and less frequency oscillations and takes less settling time. Frequency deviations in all clusters are in the range of 0.1% Hz in the presence of the proposed method. Table 2 compares the results of different controllers in terms of settling time, rise time, overshoot, and integral time absolute error (ITAE) index. From this table, it can be concluded that the proposed method can eliminate frequency deviations within 4–5 s and significantly reduce the amplitude of oscillations, which means that it better meets the requirements of microgrid frequency control. Figure 15 shows the output of the VIC controller in all three clusters.

Here, the performance of the different controllers is evaluated under high wind power penetration. Figures 16–18 show the frequency deviation of all three MG clusters. It is clear from these figures that the proposed method keeps the

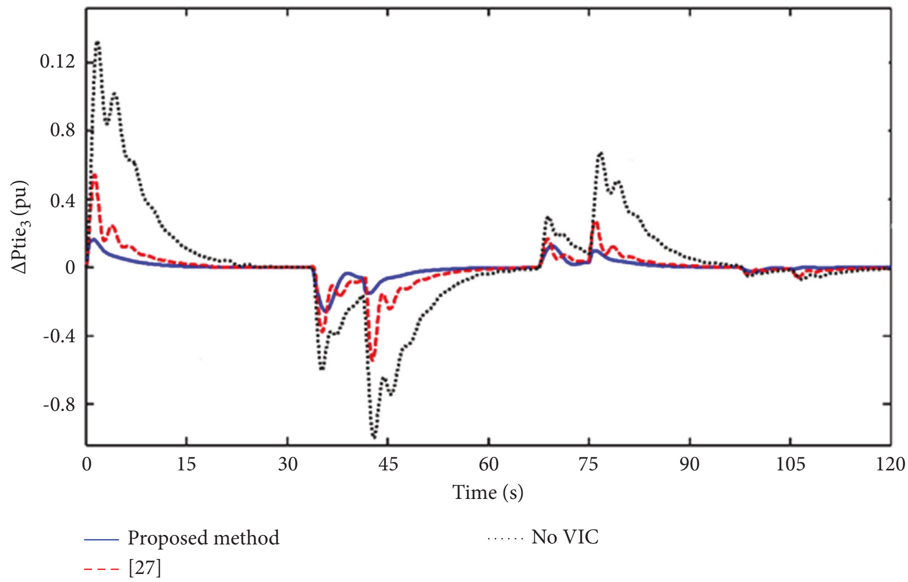

Figure 14: The tie line power deviation between cluster 1 and cluster 3.

Table 2: A comparative study between controllers.

	Settling time (s)	Rise time (s)	Overshoot (%)	ITAE
Proposed method	4.81	1.13	10.33	2.03
[6]	9.65	2.06	21.41	4.76
No VIC	14.72	2.44	31.54	6.99

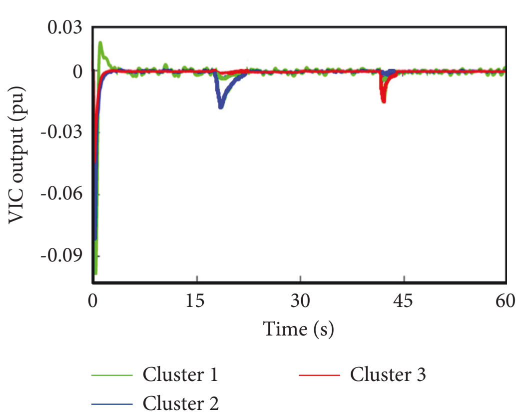

Figure 15: Output of VIC controllers at three clusters.

frequency deviation range of clusters within ± 0.15 Hz. In addition, when no virtual inertia is used, the microgrid frequency oscillates with large frequency deviations due to severe lack of inertia. The method proposed in [6] provides less inertia than the proposed VIC. Therefore, the proposed VIC can better maintain the frequency stability of low-inertia microgrid clusters.

5.2. HIL Tests. Here, real-time hardware-in-the-loop tests are used to verify the proposed μ-synthesis-based VIC. Figure 19 shows the HIL system including two section

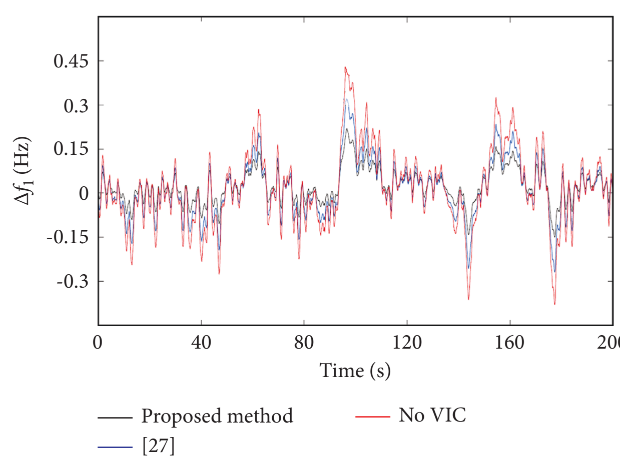

Figure 16: The frequency deviation in cluster 1.

segments: controller and physical circuits. An OP5600 real-

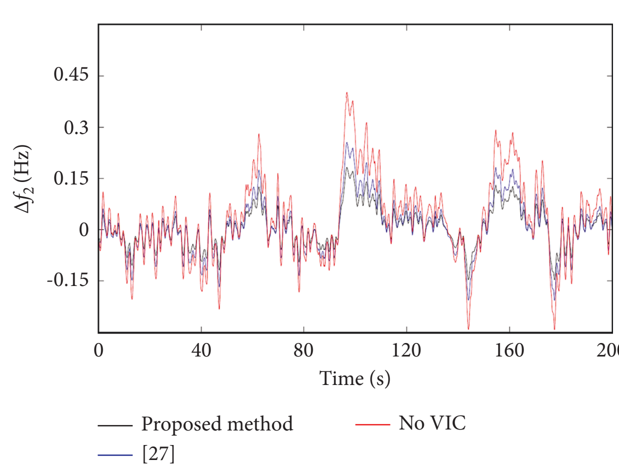

Figure 17: The frequency deviation in cluster 2.

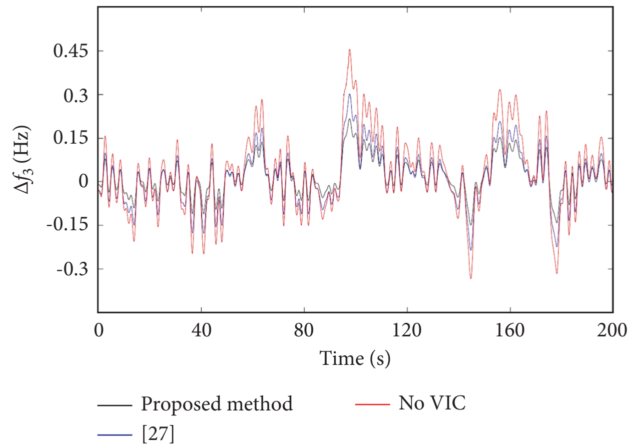

Figure 18: The frequency deviation in cluster 3.

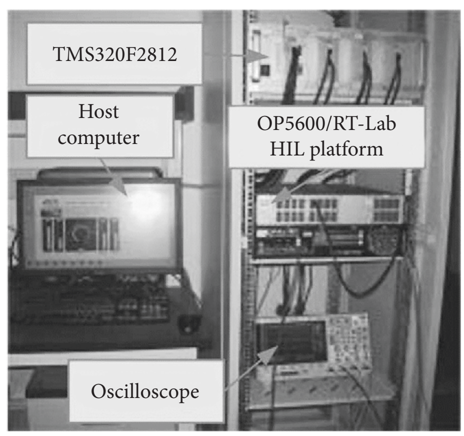

Figure 19: The HIL setup.

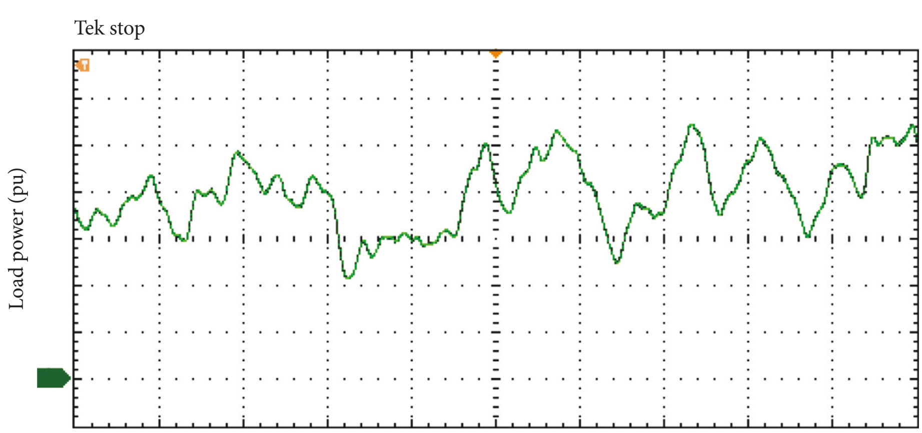

Figure 20: The load variations in cluster 1 for the HIL tests.

time simulator with time steps of 20 microseconds that can mimic the dynamics of real power components is used to realize physical circuits. The controller is implemented in a TMS320F2812 DSP processor which is programmed by the MATLAB DSP support package.

Due to hardware limitations, the HIL test is performed on the microgrid only with one cluster (cluster shown in Figure 2(a)). The HIL tests are performed primarily for two purposes. The first purpose is to demonstrate the efficiency and accuracy of the proposed VIC in a real MG. The second

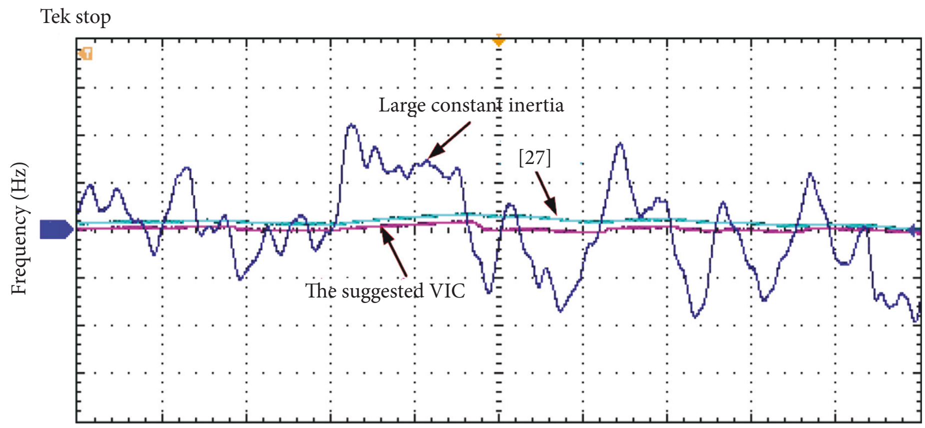

Figure 21: The HIL test results for three controllers.

Table 3: A comparative study between controllers for the HIL test.

Method	ITAE	Oscillations
The proposed method	2.39	Low
[6]	5.98	Relatively low
No VIC	33.64	High

is to evaluate the ability of the real-time computing, correctness, and robustness of the suggested controller in the real world. The total power demand in cluster 1 is shown in Figure 20. The frequency deviation in cluster 1 is illustrated in Figure 21. It is clear that when no virtual inertia is used, the microgrid frequency oscillates with large frequency deviations due to severe lack of inertia. The frequency deviation is much less when the suggested VIC is used, which means it provides more inertia compared to other methods. Therefore, the proposed VIC can better maintain the frequency stability of low-inertia microgrid clusters.

Table 3 compares the performance of three controllers in the HIL test. Clearly, considering the ITAE index, the suggested method provides the best performance.

6. Conclusion

Renewable energy resources have inherently a low inertia, since they have no rotating part. Hence, large frequency deviation occurs when the microgrid contains high-penetration RESs. This paper suggests virtual inertia control to enhance the inertia of renewable energy resources in islanded microgrid clusters considering high RES penetration, uncertainties, and nonlinearities. To achieve robust and optimal VIC and to decrease the impact of dynamic perturbations and uncertainties, a μ-synthesis method is used. In the structure of the suggested VIC, there are both the inertial response characteristics of original synchronous generator and the fast dynamics of power electronic interfaces. The suggested method can compensate the lack of inertia in the MG clusters. As discussed, robust controllers are designed to reduce the impacts of wind farm, photovoltaic, and load disturbances and dynamic perturbations. It is shown that in the case of using the structured uncertainty (μ approach), the obtained controller demonstrates better performance. It is demonstrated that in the case of utilizing the structured uncertainty, the controller shows a satisfactory performance. Islanded microgrid clusters are utilized to confirm the efficiency of the suggested VIC. The simulation and HIL results confirm that the suggested controller can reduce the frequency deviations considerably and also show superior performance of the suggested VIC in the presence of high RES penetration and heavy loading.

Data Availability

No data were used to support this study.

Conflicts of Interest

The authors declare that they have no conflicts of interest.

References

[1] A. M. Othman and A. A. El-Fergany, "Design of robust model predictive controllers for frequency and voltage loops of interconnected power systems including wind farm and energy storage system," *IET Generation, Transmission & Distribution*, vol. 12, no. 19, pp. 4276–4283, 2018.

[2] H. M. Hasanien and A. A. El-Fergany, "Symbiotic organisms search algorithm for automatic generation control of interconnected power systems including wind farms," *IET Generation, Transmission & Distribution*, vol. 11, no. 7, pp. 1692–1700, 2017.

[3] M. A. El-Hameed, M. M. Elkholy, and A. A. El-Fergany, "Efficient frequency regulation in highly penetrated power systems by renewable energy sources using stochastic fractal optimiser," *IET Renewable Power Generation*, vol. 13, no. 12, pp. 2174–2183, 2019.

[4] J. Liu, Y. Miura, and T. Ise, "Comparison of dynamic characteristics between virtual synchronous generator and droop control in inverter-based distributed generators," *IEEE*

Transactions on Power Electronics, vol. 31, no. 5, pp. 3600–3611, 2016.
[5] C. Pradhan, C. N. Bhende, and A. K. Samanta, "Adaptive virtual inertia-based frequency regulation in wind power systems," *Renewable Energy*, vol. 115, pp. 558–574, 2018.
[6] M. Hajiakbari Fini and M. E. Hamedani Golshan, "Determining optimal virtual inertia and frequency control parameters to preserve the frequency stability in islanded microgrids with high penetration of renewables," *Electric Power Systems Research*, vol. 154, pp. 13–22, 2018.
[7] C. Chen, K. Zhang, J. Geng, K. Yuan, Z. Yang, and L. Li, "Multiobjective-based optimal allocation scheme for load frequency control," *International Transactions on Electrical Energy Systems*, vol. 27, no. 7, Article ID e2334, 2017.
[8] M. A. Mohamed, A. A. Z. Diab, H. Rezk, and T. Jin, "A novel adaptive model predictive controller for load frequency control of power systems integrated with DFIG wind turbines," *Neural Computing & Applications*, vol. 32, no. 11, pp. 7171–7181, 2020.
[9] W. Wu, Y. Chen, A. Luo et al., "A virtual inertia control strategy for DC microgrids analogized with virtual synchronous machines," *IEEE Transactions on Industrial Electronics*, vol. 64, no. 7, pp. 6005–6016, 2017.
[10] Y. Li, Z. Xu, and K. P. Wong, "Advanced control strategies of PMSG-based wind turbines for system inertia support," *IEEE Transactions on Power Systems*, vol. 32, no. 4, pp. 3027–3037, 2017.
[11] Y. Wang, J. Meng, X. Zhang, and L. Xu, "Control of PMSG-based wind turbines for system inertial response and power oscillation damping," *IEEE Transactions on Sustainable Energy*, vol. 6, no. 2, pp. 565–574, 2015.
[12] H. Ye, W. Pei, and Z. Qi, "Analytical modeling of inertial and droop responses from a wind farm for short-term frequency regulation in power systems," *IEEE Transactions on Power Systems*, vol. 31, no. 5, pp. 3414–3423, 2016.
[13] B. S. Solaiappan and K. Nagappan, "AGC for multisource deregulated power system using ANFIS controller," *International Transactions on Electrical Energy Systems*, vol. 27, no. 3, Article ID e2270, 2017.
[14] M. Moafi, M. Marzband, M. Savaghebi, and J. M. Guerrero, "Energy management system based on fuzzy fractional order PID controller for transient stability improvement in microgrids with energy storage," *International Transactions on Electrical Energy Systems*, vol. 26, no. 10, pp. 2087–2106, 2016.
[15] P. Dahiya, V. Sharma, and R. Naresh, "Optimal sliding mode control for frequency regulation in deregulated power systems with DFIG-based wind turbine and TCSC–SMES," *Neural Computing & Applications*, vol. 31, no. 7, pp. 3039–3056, 2019.
[16] J. Van de Vyver, J. D. M. De Kooning, B. Meersman, L. Vandevelde, and T. L. Vandoorn, "Droop control as an alternative inertial response strategy for the synthetic inertia on wind turbines," *IEEE Transactions on Power Systems*, vol. 31, no. 2, pp. 1129–1138, 2016.
[17] X. Yuan and Y. Li, "Control of variable pitch and variable speed direct-drive wind turbines in weak grid systems with active power balance," *IET Renewable Power Generation*, vol. 8, no. 2, pp. 119–131, 2014.
[18] T. Kerdphol, F. S. Rahman, Y. Mitani, M. Watanabe, and S. Kufeoglu, "Robust virtual inertia control of an islanded microgrid considering high penetration of renewable energy," *IEEE Access*, vol. 6, pp. 625–636, 2018.
[19] T. Kerdphol, M. Watanabe, K. Hongesombut, and Y. Mitani, "Self-adaptive virtual inertia control-based fuzzy logic to improve frequency stability of microgrid with high renewable penetration," *IEEE Access*, vol. 7, pp. 76071–76083, 2019.
[20] J. Li, B. Wen, and H. Wang, "Adaptive virtual inertia control strategy of VSG for micro-grid based on improved bang-bang control strategy," *IEEE Access*, vol. 7, pp. 39509–39514, 2019.
[21] J. Meng, Y. Wang, C. Fu, and H. Wang, "Adaptive virtual inertia control of distributed generator for dynamic frequency support in microgrid," in *Proceedings of the 2016 IEEE Energy Conversion Congress and Exposition (ECCE)*, IEEE, Milwaukee, WI, USA, September 2016.
[22] D. C. Das, A. K. Roy, and N. Sinha, "GA based frequency controller for solar thermal–diesel–wind hybrid energy generation/energy storage system," *International Journal of Electrical Power & Energy Systems*, vol. 43, no. 1, pp. 262–279, 2012.
[23] D. C. Das, N. Sinha, and A. K. Roy, "Automatic generation control of an organic rankine cycle solar–thermal/wind–diesel hybrid energy system," *Energy Technology*, vol. 2, no. 8, pp. 721–731, 2014.
[24] K. M. Singh and S. Gope, "Renewable energy integrated multi-microgrid load frequency control using grey wolf optimization algorithm," *Materials Today Proceedings*, vol. 46, pp. 2572–2579, 2021.
[25] B. P. Sahoo and S. Panda, "Load frequency control of solar photovoltaic/wind/biogas/biodiesel generator based isolated microgrid using Harris Hawks optimization," in *Proceedings of the 2020 First International Conference on Power, Control and Computing Technologies (ICPC2T)*, IEEE, Raipur, India, January 2020.
[26] K. M. Singh, S. Gope, and N. Pradhan, "Firefly algorithm-based optimized controller for frequency control of an autonomous multi-microgrid," in *Proceedings of the International Conference on Innovative Computing and Communications*, Springer, Singapore, January 2021.
[27] H. Bevrani, M. R. Feizi, and S. Ataee, "Robust frequency control in an islanded microgrid: H∞ and μ-synthesis approaches," *IEEE Transactions on Smart Grid*, vol. 7, no. 2, pp. 1–717, 2015.
[28] V. Natarajan and G. Weiss, "Synchronverters with better stability due to virtual inductors virtual capacitors and anti-windup," *IEEE Transactions on Industrial Electronics*, vol. 64, no. 7, pp. 5994–6004, 2017.
[29] H. Bevrani, T. Ise, and Y. Miura, "Virtual synchronous generators: a survey and new perspectives," *International Journal of Electrical Power & Energy Systems*, vol. 54, pp. 244–254, 2014.
[30] R. Hesse, D. Turschner, and H. Beck, "Micro grid stabilization using the virtual synchronous machine (VISMA)," in *Proceedings of the ICREPQ'09*, Valencia, Spain, 2009.
[31] J. Driesen and K. Visscher, "Virtual synchronous generators," in *Proceedings of the 2008 IEEE Power and Energy Society General Meeting - Conversion and Delivery of Electrical Energy in the 21st Century*, Pittsburgh, PA, USA, July 2008.
[32] Y. Hirase, K. Abe, K. Sugimoto, and Y. Shindo, "A grid-connected inverter with virtual synchronous generator model of algebraic type," *Electrical Engineering in Japan*, vol. 184, no. 4, pp. 10–21, 2013.
[33] A. Packard and J. Doyle, "The complex structured singular value," *Automatica*, vol. 29, no. 1, pp. 71–109, 1993.